The Influence of Island Topography on Typhoon Track Deflection

YI-HSUAN HUANG AND CHUN-CHIEH WU

Department of Atmospheric Sciences, National Taiwan University, Taipei, Taiwan

YUQING WANG

International Pacific Research Center, and Department of Meteorology, University of Hawaii at Manoa, Honolulu, Hawaii

(Manuscript received 2 July 2010, in final form 10 January 2011)

ABSTRACT

High-resolution simulations for Typhoon Krosa (2007) and a set of idealized experiments are conducted using a full-physics model to investigate the eminent deflection of typhoon track prior to its landfall over mountainous island topography. The terrain height of Taiwan plays the most important role in Typhoon Krosa's looping motion at its landfall, while the surface properties, details in the topographic shape of Taiwan, and the cloud microphysics are shown to be secondary to the track deflection. A simulation with 3-km resolution and realistic model settings reproduces the observed Krosa's track, while that with 9-km resolution fails, suggesting that high resolution to better resolve the typhoon–terrain interactions is important for the prediction and simulation of typhoon track deflection prior to landfall. Results from idealized experiments with model configurations mimicking those of Supertyphoon Krosa show that vortices approaching the northern and central topography are significantly deflected to the south before making sharp turns to the north, forming a kinked track pattern prior to and during landfall. This storm movement is consistent with the observed looping cases in Taiwan.

Both real-case and idealized simulations show strong channel winds enhanced between the storm and the terrain when deflection occurs. Backward trajectory analyses support the concept of the channeling effect, which has been previously found to be crucial to the looping motion of Typhoon Haitang (2005) as well. However, the inner-core asymmetric ventilation flow does not match the movement of a deflected typhoon perfectly, partly because the steering flow is not well defined and could not completely capture the terrain-induced deflection in the simulation and in nature.

1. Introduction

Located in the western North Pacific, Taiwan suffers from 3 to 6 typhoons each year. The severe wind gusts and heavy rain associated with a typhoon often lead to major catastrophes, making typhoons one of the most serious meteorological phenomena. Taiwan is a mountainous area with complex terrain features, including plains in the west and rugged mountains running in five ranges from the northern to the southern tips of the island. Particularly noteworthy is the Central Mountain Range (CMR) with an average elevation of 2000 m and a peak close to 4000 m. These exceptionally high ranges can cause significant changes in typhoon tracks and intensity, and the accompanying rainfall patterns. Furthermore, the intricacies of the terrain shape lead to highly variable precipitation distributions over Taiwan. Although many previous studies have investigated this topic, the quantitative results are not consistent. Besides, significant track deflection prior to landfall has been little addressed in the literature. Apparently, topographic impacts on typhoons indigenous to Taiwan make typhoon forecasting very challenging. Terrain-induced tropical cyclone (TC) evolution, including track, intensity, structure, and the associated rainfall, depends primarily on how a TC approaches the topography. Accordingly, the influence of the topography on track deflection, sharp turns in particular, is regarded as a priority for investigation.

Both observational and numerical studies have shown that typhoons are prone to being deflected when approaching Taiwan. Earlier related studies have been

Corresponding author address: Chun-Chieh Wu, Dept. of Atmospheric Sciences, National Taiwan University, No. 1, Sec. 4, Roosevelt Rd., Taipei 106, Taiwan.
E-mail: cwu@typhoon.as.ntu.edu.tw

DOI: 10.1175/2011MWR3560.1

reviewed in detail by Wu and Kuo (1999). Observations showed that westbound typhoons tend to move cyclonically around the northern side of the CMR (e.g., Brand and Blelloch 1974; Wang 1980; Chang 1982). Wang (1980) indicated that this might be due to the deflection of the mean steering flow upstream of the CMR. To further understand the influence of topography on TC tracks, numerical simulations have been employed as well (e.g., Chang 1982; Bender et al. 1987; Wu 2001; Yeh and Elsberry 1993a,b; Lin et al. 1999, 2005). Chang (1982) found that mountain-induced deflection of steering flow is confined to the lower levels. Idealized experiments conducted by Yeh and Elsberry (1993a,b) showed that the track deflection could be larger for the case of weaker and slower-moving storms, which is consistent with the findings of real-case simulations conducted by Bender et al. (1987). A cyclonic track (northwestward deflection around the upstream of the terrain) induced by Taiwan's topography was captured in a simulation of Typhoon Gladys by Wu (2001). Using a full-physics model, Yeh and Elsberry (1993a) designed a series of idealized experiments with model resolution of 45 km. They found that vortices approaching the southern portion of the barrier were deflected to the south in a region approximately between 250 and 400 km upstream of the barrier (region B in their Figs. 13 and 22), while those approaching the central and northern portion were slightly deflected to the north or not deflected (see their Fig. 12). By subtracting the deflection from the influence of the basic flow (deep-layer mean flow in their barrier control experiment), Yeh and Elsberry (1993a) examined the deflection without contribution from the terrain-modified basic flow. Based on the analyses of the asymmetric structure and the ventilation flow, Yeh and Elsberry (1993a) speculated that the channeling effect may drift a vortex southward (relative to the steering of the basic flow) to the topography over region B. The channeling effect occurs when flow passes the narrow space between the barrier and the inner-core vortex, where the inertial stability is strong enough to be a virtual barrier. When getting closer to the topography (250 km upstream of the terrain, region C in their Figs. 13 and 22), the storm motion behaved differently; vortices approaching the southern part of the barrier were initially deflected northward, while those approaching the northern end were only slightly influenced. Yeh and Elsberry (1993a) found that it was the terrain-induced imbalance of the inner-core structure that led to the northward turn. Winds to the west of the storm were weakened by the topography, in particular for those approaching the southern part of the barrier because the cyclonic circulation impinged onto a wider area of the topography. Hence, significant southerly asymmetric flow in the inner-core region is generated, and may drift the vortex northward prior to landfall (region C). Although Yeh and Elsberry (1993a) stressed the importance of the terrain-induced inner-core imbalance in leading to the deflection, the inner-core structure was not resolved well with the coarse model resolution (45 km).

More recently, Lin et al. (2005) conducted idealized simulations with much higher resolution, but without moist physics and the effect of surface friction. They introduced six nondimensional parameters for TC track deflection inferred from previous studies. These parameters are $V_{\max}/Nh$, U/Nh, $V_{\max}/fR$, U/fL_x, h/L_x, and R/L_y; namely, the Froude numbers of the vortex and the basic flow, the Rossby numbers of the vortex and the basic flow, the steepness of the topography, and the ratio of the vortex size to the barrier scale in the y direction, respectively. Here the y direction is normal to the movement of the vortex. Consistent with the earlier observational and numerical studies, most of their simulations showed that vortices are deflected northward prior to landfall. Greater track variations occur in the simulations with smaller Froude numbers of the vortex and the basic flow, ratio of the vortex size to the barrier scale (y direction), Rossby numbers of the vortex and the basic flow, and with steeper topography. Nevertheless, southward deflection occurs under a specific condition, which is the combination of extremely small values of $V_{\max}/Nh$, U/Nh, $V_{\max}/fR$, U/fL_x, and R/L_y, and a very large value of h/L_x. However, this southward track deflection has rarely been found in the earlier observations (Brand and Blelloch 1974) or numerical studies (e.g., Chang 1982; Bender et al. 1987; Yeh and Elsberry 1993a). The difference between the results of Yeh and Elsberry (1993a) and Lin et al. (2005) implies that high-resolution full-physics models may be crucial to the study of terrain-induced track deviations. Wu and Kuo (1999) and Wu (2001) also showed the importance of typhoon initialization and moist processes for track prediction. Although a number of idealized numerical studies have been conducted to simulate the track deflections, few of them were based on a full-physics model with high model resolution. Therefore numerical studies with full-physics high-resolution models are indispensable for investigating the dynamics of the terrain-induced track deflection.

In some cases, tracks can be dramatically deflected by topography, causing a looping motion [e.g., Shirley (1960), Mary (1965), Sarah (1989), Polly (1992), Haitang (2005), Krosa (2007), and Sinlaku (2008)]. Areas lashed by severe rainfall and gusts can be shifted greatly because of sharp turns, bringing about one of the important typhoon forecasting problems. However, such unusual motion has not been well addressed in the literature.

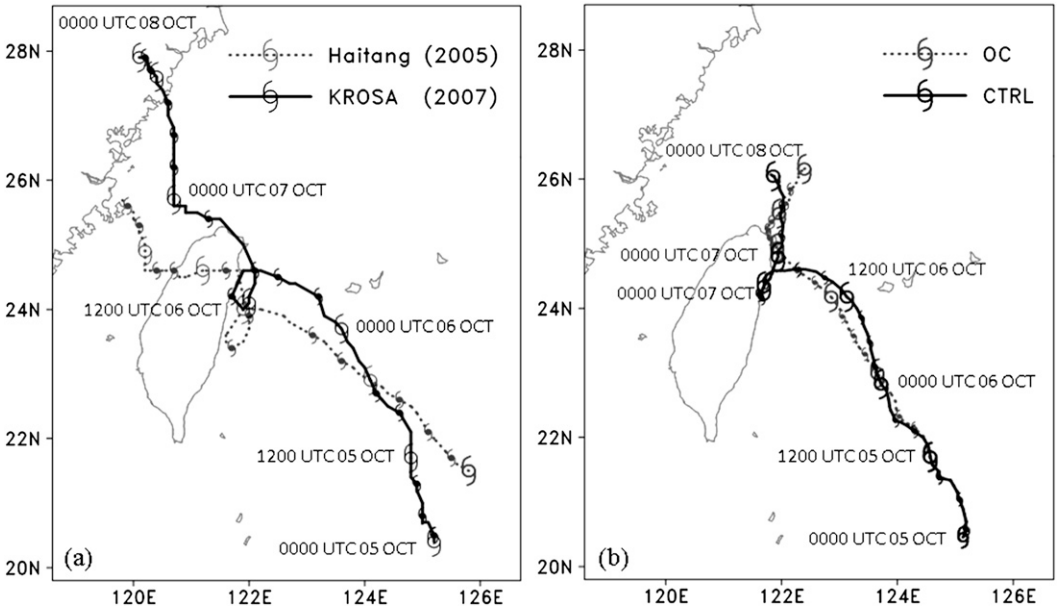

FIG. 1. (a) CWB's best track of Haitang (2005) and Krosa (2007) with hourly temporal resolution from 0000 UTC 17 Oct to 0600 UTC 19 Oct and from 0000 UTC 5 Oct to 0000 UTC 8 Oct, respectively. (b) CTRL and OC for Krosa in this paper. The solid typhoon symbols refer to the centers at 0300, 0600, 0900, 1500, and 1800 UTC while the open typhoon symbols denote those at 0000 and 1200 UTC. The corresponding time is also indicated beside each typhoon symbol at 0000 and 1200 UTC.

Supertyphoon Haitang (2005) is one of the few cases that have been studied. Jian and Wu (2008) investigated the physical processes responsible for Haitang's significant track deflection and looping motion. The cyclonic loop was well captured in their simulation. They showed that high terrain played a critical role in inducing the strong low-level northerly jet to the west of Haitang (i.e., the channeling effect, e.g., Lin et al. 1999; 2005) and, thus, the northerly flow deflected the typhoon southward. When Haitang moved closer to the topography, winds to the west of the typhoon center weakened significantly by the high barrier. Then, southerly asymmetric flow in the inner-core region was induced, and it steered Haitang to the north. Therefore, Haitang made a loop during this period. The explanation for Haitang's looping motion is similar to that of the track deflection (both southward and northward) reported in Yeh and Elsberry (1993a). However, the regions where the deflection occurs differ greatly. The southward deflection in Yeh and Elsberry (1993a) was located between 250 and 400 km upstream of the barrier, while those for the observed Haitang and Krosa, and the simulated Haitang in Jian and Wu (2008) were present within 100 km upstream of the Taiwan topography. Besides, although both of the southward turns are attributed to the channeling effect, the channeling effect is suggested to have influence on the storm's wind field at different radii, that is, over the outer circulation in Yeh and over Elsberry (1993a) and over the inner-core region in Jian and Wu (2008). Another important discrepancy is that topography had a weak influence on the tracks of the intense vortices in Yeh and Elsberry (1993a), while Haitang, a supertyphoon, can be significantly deflected by topography. This suggests that the physical processes leading to the typhoon track deflection in models with different resolutions are likely very different.

After Haitang, Krosa (2007) is another case with looping motion, providing an opportunity for further investigation of such unusual movement. Haitang and Krosa are both supertyphoons that moved northwestward when approaching Taiwan with a similar translational speed before making a loop. However, their looping motion occurred in different regions. Haitang made a loop as its center was near the central part of Taiwan, while Krosa made a loop as it was moving around the northern part of Taiwan (Fig. 1a). It is thus unclear if the dynamics involved in the looping motion of Krosa is the same as that in Haitang and if the Taiwan topography plays a critical role in Krosa's looping motion as well. Based on the typhoon database constructed by the Central Weather Bureau (CWB, Taiwan), around 41 westbound typhoons were documented as supertyphoons between 1958 and 2010 near the Taiwan topography, and 7 of them underwent significant southward turn or looping motion prior to their landfall over Taiwan. In all, eight typhoons have been documented

with this unique motion prior to landfall. Except typhoon Polly, all these typhoons are supertyphoons (>51 m s^{-1}). This suggests that it is important to investigate the topographic influence on tracks of intense typhoons. Furthermore, idealized numerical studies have rarely addressed terrain-induced looping or sharp southward deflection prior to or during landfall, especially little for an intense typhoon and for simulations based on a full-physics model with fine resolutions. Note that Yeh and Elsberry (1993a) carried out simulations with a coarse model resolution (45 km). Hence, in the model the vortices are rather weak, while the terrain height was much lower with broader size. More recently, Lin et al. (2005) performed idealized simulations with much finer resolution to study this issue, but diabatic processes and the impact of surface friction were excluded in their model. With these concerns, to systematically examine the terrain-induced track deflection, we performed idealized experiments with topographic size and height similar to that of Taiwan with vortex intensity and size similar to typhoons like Haitang and Krosa, and with different initial vortex locations. To conduct more realistic simulations, a full-physics model with fine horizontal resolution is utilized.

The objectives of this study are threefold: 1) to investigate the mechanisms leading to the looping motion of Typhoon Krosa (2007), 2) to examine how the motion of an idealized vortex in a uniform flow responds when the vortex encounters an idealized topography, and 3) to indentify parameters and flow regimes that lead to typhoon track deflection by conducting idealized experiments using a high-resolution full-physics model. The rest of the paper is organized as follows. Section 2 gives a brief overview of Supertyphoon Krosa. Section 3 describes the model setup and experimental design for both the real-case simulation of Krosa and the idealized simulations. The numerical results of Krosa and idealized simulations are discussed in sections 4 and 5, respectively. The main findings are summarized in section 6 together with a discussion of some remaining issues.

2. An overview of Supertyphoon Krosa (2007)

Krosa intensified into a supertyphoon at 1200 UTC 4 October while it was located approximately 600 km southeast of Taiwan's southern tip. At the same time, it reached its peak intensity with an estimated maximum sustained wind of 51 m s^{-1} (10-min mean of the 10-m wind) and a minimum sea level pressure of 925 hPa, with a 300-km radius of 15-m s^{-1} wind. As shown in Fig. 1a, Krosa moved northwestward from 0000 UTC 5 October to 0300 UTC 6 October, and then headed west during the following 4 h. After that, Krosa turned to the south and moved along the shoreline for 50 km in 2 h. It made landfall at the northern tip of Taiwan at around 1500 UTC 6 October. Then, it began to veer to a northward track at 1100 UTC 6 October. Namely, Krosa made a cyclonic loop between 0700 and 1400 UTC 6 October. Doppler radar observations (not shown) documented the sharp southward turn and the slow cyclonic loop off the northern east coast of Taiwan between 0700 and 1400 UTC 6 October. During this period, the maximum sustained wind had decreased from 51 to 45 m s^{-1} and the minimum sea level pressure increased from 925 to 940 hPa according to the analyses from CWB. Thereafter, Krosa moved toward the northwest again and quickly passed over the northeast coast in about 2 h. Finally, it turned to the north at 2300 UTC 6 October, and made landfall over mainland China at 0900 UTC 7 October with a maximum wind of 23 m s^{-1}. Although Krosa's center remained within Taiwan Island for only 2 h, the 7-h looping motion near the coast led to heavy rain and strong winds over Taiwan.

3. Model and experimental design

All of the numerical simulations are based on the fifth-generation Penn State University–National Center for Atmospheric Research (PSU–NCAR) Mesoscale Model (MM5, version 3.7.3; Grell et al. 1995). The nonhydrostatic MM5 with full physics is used to perform 72-h simulations. The horizontal resolutions of the three nest domains are 27, 9, and 3 km, respectively, and the resolutions of the terrain and land-use data for these domains are 10, 5, and 2 min (about 19, 9, and 4 km), respectively. The model vertical levels extend from the surface to 10 hPa and are divided into 32 layers (1.00, 0.997, 0.995, 0.992, 0.99, 0.985, 0.98, 0.975, 0.97, 0.965, 0.96, 0.95, 0.93, 0.89, 0.85, 0.80, 0.75, 0.70, 0.65, 0.60, 0.55, 0.50, 0.45, 0.40, 0.35, 0.30, 0.25, 0.20, 0.15, 0.10, 0.05, and 0.00) in the terrain-following σ coordinate [$\sigma = (p - p_t)/(p_s - p_t)$, where p_s is surface pressure, p denotes pressure, and p_t is the pressure at the model top and is set to be 10 hPa].

The high-resolution Blackadar planetary boundary layer (PBL) scheme (Blackadar 1976, 1979; Zhang and Anthes 1982), the simple ice scheme of Dudhia (1989) and the simple longwave radiation cooling scheme are adopted for all meshes. The Grell cumulus parameterization is utilized only in the coarsest mesh but not in the two inner nested meshes since the grid sizes could resolve convection reasonably well. All of the above settings are applied to both the real-case and the idealized simulations, while the settings for the horizontal domain sizes are different. The respective domain sizes for the simulation of Krosa's and the idealized runs will be introduced in sections 3a and b, respectively.

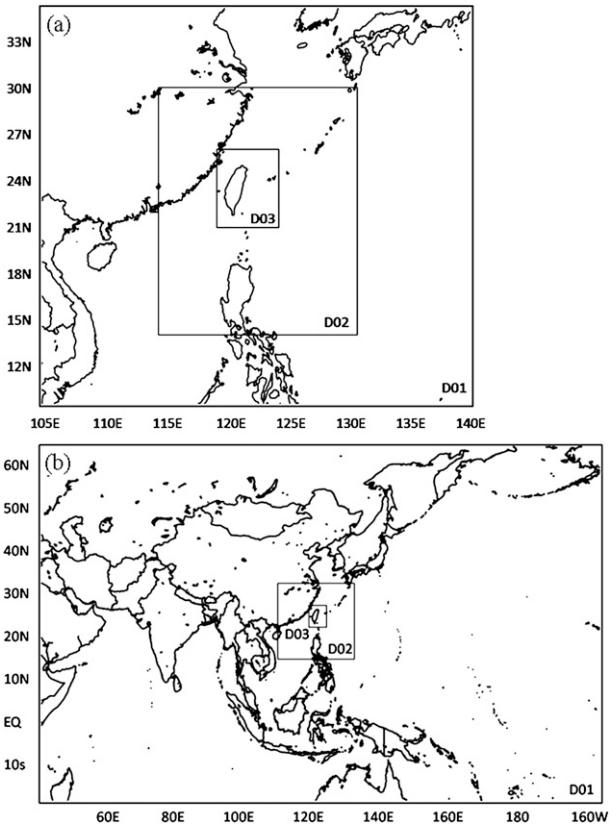

FIG. 2. Model domains D01, D02, and D03 used, respectively, in (a) Krosa and (b) the idealized experiments.

a. Typhoon Krosa

The initial and lateral boundary conditions are based on the National Centers for Environmental Prediction (NCEP) Global Forecast System (GFS) global final analysis data (1° × 1°). The initial time is 0000 UTC 5 October 2007. The horizontal dimensions of the 3 domains (Fig. 2a) are 112 × 121, 208 × 208, and 190 × 172, respectively. The model initialization and vortex bogusing are based on the method described in Wu et al. (2002). The minimum sea level pressure, the maximum wind speed at the lowest model level, and the radius of 15-m s^{-1} wind of the initial vortex are 927 hPa, 45 m s^{-1}, and 300 km, respectively (Fig. 3). Moreover, the vertical cross sections of the initial tangential wind and potential temperature (Fig. 3b) demonstrate a reasonable inner core structure, including a warm core in the typhoon eye region and a compact eyewall. As a result, the simulated vortex strength and structure are comparable to those of Krosa at this moment. To reduce the computation time, the finest mesh is activated after 22 h of integration when the outer circulation of Krosa is about to impinge the Taiwan terrain in the simulations. After this mesh is activated, Krosa keeps intensifying, and the maximum wind reaches about 56 m s^{-1}, which is about 5 m s^{-1} stronger than that observed prior to the landfall over Taiwan. Meanwhile, the radius of 15-m s^{-1} wind is approximately 300 km, consistent with the analyses from CWB. These TC properties suggest that the overall structure and intensity evolution in the simulation agrees with the observation before the outer circulation of Krosa is influenced by Taiwan topography.

Topography influences the typhoon motion via the terrain height and the surface properties (ocean or land). To clarify the role of the island's terrain height in Krosa's sharp turn, five experiments are conducted: H70, H40, H10, FT, and H130 (see Table 1). Then, two experiments (OC and OCH) are carried out with underlying ocean conditions to investigate the impacts of the surface properties. Among these experiments, H70, H40, and H10 are the same as those in Jian and Wu (2008). Meanwhile, FT and OC are the same as FLAT and NT in Jian and Wu (2008). To evaluate the importance of model resolution, a simulation (R09) is run without activating the third mesh (i.e., with the finest resolution of 9 km). In addition, because the life cycle of a typhoon in a numerical simulation can be sensitive to the selected model physics, an experiment [the Reisner Graupel scheme (RGRP)] is performed to examine the response of Krosa to Taiwan's topography by using a different and more sophisticated cloud microphysics scheme (Reisner 2). The control experiment, named CTRL, retains all of the model-resolved terrain. Details of all experiments are described in Table 1.

b. Idealized experiments

All of the idealized experiments are conducted on the *f* plane so as to exclude the impact of beta effect on the typhoon track. The horizontal dimensions of the 3 domains are 337 × 487, 223 × 259, and 211 × 166 grid points, respectively (Fig. 2b). We set a large outermost domain to minimize any effects of the fluctuations and disturbances around the lateral boundary on the vortex.

The initialization of the idealized simulations is done in the outermost domain. The initialization procedure follows that in Huang et al. (2008). The nonlinear balance equation (Charney 1955; Wu et al. 2003b) and fixed lateral boundary conditions are employed. Mean West Indies sounding data for hurricane season (July–October) in Jordan (1958, their Table 5) are utilized as the reference state of the initial fields, including pressure, height, temperature, and relative humidity. The idealized vortex (DeMaria and Chan 1984) is defined as

$$V' = V_{\max}\frac{r}{r_{\max}}\exp\left\{\frac{1}{b}\left[1-\left(\frac{r}{r_{\max}}\right)^{b}\right]\right\}, \qquad (1)$$

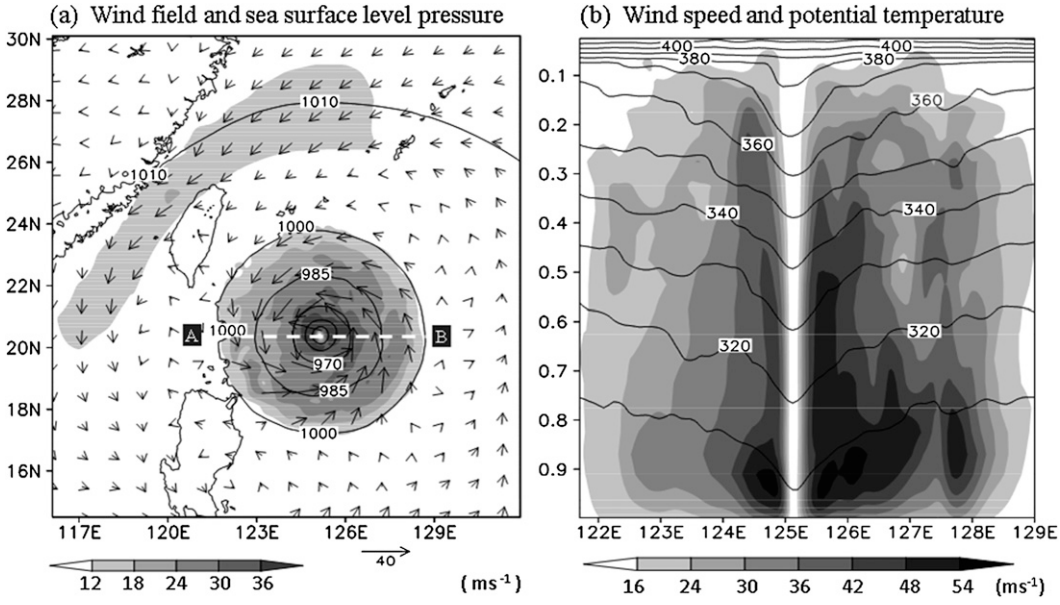

FIG. 3. The initial field of Krosa in CTRL. (a) Winds (wind field: arrows, wind speed: shadings) at the lowest model level, and sea surface level pressure (contours); (b) the vertical cross sections of the initial tangential wind (shadings) and the potential temperature (contours) along the A–B line (white dashed) in (a).

where V_{max} is the maximum tangential wind speed, r_{max} is the radius of maximum wind (RMW), and b is a factor determining the rate at which the tangential wind decays with radius. V_{max}, r_{max}, and b are specified as 35 m s^{-1}, 50 km, and 0.5, respectively. A 5 m s^{-1} easterly basic flow is used in all of the idealized experiments, which is about the averaged environmental flow of Krosa and leads to a translational speed of the vortex comparable to that of Krosa.

The idealized bell-shaped topography (Lin et al. 1999) is prescribed as

$$h(x, y) = \frac{h_{max}}{\left[\left(\frac{x}{a}\right)^2 + \left(\frac{y}{b}\right)^2 + 1\right]^{3/2}}, \quad (2)$$

where h is the mountain height, h_{max} is the maximum mountain height, and a and b stand for the mountain half-widths in x and y directions, respectively. To better characterize the topography, we reformulate Eq. (2) as

$$h(x, y) = \frac{H'}{\left[\left(\frac{x - x_c}{a}\right)^2 + \left(\frac{y - y_c}{b}\right)^2 + 1\right]^{3/2}} - h', \quad (3)$$

where $h' = H'/2^{3/2}$, so that the edge of the topography will be 0. Here H' is determined by the maximum terrain height, defined as $H' = 8/7[1 + 1/2^{3/2})]h_{max}$. The h_{max} is 3000 m, which is comparable to the average height of the CMR's peaks. In addition, a and b are 75 and 200 km, respectively. Based on the above settings, we can construct a terrain similar to that of Taiwan. x_c and y_c denote the longitude and latitude of the terrain's central position, referring to Taiwan's central position at 23.5°N, 121.1°E.

Inspired by the experiments performed by Yeh and Elsberry (1993a), two groups of experiments are designed for the idealized simulations. One group uses only the ocean surface, denoted as "OC." The other uses the aforementioned bell-shaped terrain, denoted as "H." Nine experiments with varying initial latitudinal positions of the vortex center are conducted in each group, where "xn" and "xs" are used to denote the initial positions of the vortices. Here "n" and "s" refer to "north" and "south," indicating that a vortex is to the north or south

TABLE 1. Description of experiments for Krosa.

Expt	Topography in Taiwan	Resolution
CTRL	Full topography	27/9/3 km
OC	Ocean	As in CTRL
H10	10% of the CTRL	As in CTRL
H40	40% of the CTRL	As in CTRL
H70	70% of the CTRL	As in CTRL
H130	130% of the CTRL	As in CTRL
FT	Flat topography (0.1 m high)	As in CTRL
OCH	Full topography, ocean surface	As in CTRL
RGRP	Reisner graupel (Reisner2 scheme)	As in CTRL
R09	As in CTRL	27/9 km
ITP	Bell shaped	As in CTRL

TABLE 2. Designs of the idealized experiments (x = 1, 2, 3, 4).

Name	Topography	Initial lat of the vortex center
OCxn	Ocean	23.5 + 0.5x
OC	Ocean	23.5
OCxs	Ocean	23.5 − 0.5x
Hxn	Bell shaped (as in ITP)	23.5 + 0.5x
H	Bell shaped (as in ITP)	23.5
Hxs	Bell shaped (as in ITP)	23.5 − 0.5x

of the central position of the topography. Here "x" is a number used to denote the latitudinal distance of a vortex from the central latitude of the terrain (23.5°N). The initial longitude of the vortex center in all the experiments is specified as 125.0°E. We can expect that the vortex structure is not influenced by the topography at the initial time. Through these experiments, we attempt to examine how a vortex in the uniform flow responds when it approaches different parts of the topography. Details of the idealized experimental design are shown in Table 2.

To obtain a more reasonable and balanced initial condition in the model, we perform preruns to spin up the model vortex and to adjust the basic flow separately. The idealized vortex embedded in a quiescent ambient field without topography is run for 72 h. Meanwhile, 2 runs with the uniform basic flow but with no vortex are performed for 84 h. One is with topography presented and the other with no topography. In the run with only basic flow and topography, the basic flow is deflected by the topography; the flow over the northern part is deflected to the north, while that over the southern part is to the south (figures not shown). Additionally, a clear lee vortex is present in this simulation (not shown), consistent with the findings in the previous studies (e.g., Smolarkiewicz and Rotunno 1989; Smith 1989.) After the preruns are completed, the idealized initial field is constructed by implanting the spunup idealized vortex into a particular position in the prerun basic flow, as shown in Table 2. The superposition of the vortex on the basic flow with topography gives the initial conditions for the H group; in contrast, the superposition of the vortex on the basic flow without topography gives the initial field for the OC group. The initial field is shown in Fig. 4, demonstrating a quasi-symmetric structure. The maximum wind speed at the lowest model level and the radius of 15-m s^{-1} wind of the initial vortex are 45 m s^{-1} and 250 km, respectively. The vertical profile of the initial vortex in the idealized experiments is shown in Fig. 4b.

4. Results of Supertyphoon Krosa

a. Experiment CTRL

Overall, CTRL captures the movement of Krosa, including the cyclonically curving northwestward motion when Krosa approaches Taiwan, the sharp southward deflection prior to landfall, and the sudden northward turn after its landfall (Figs. 1b and 5a). However, there are some deviations from the observed movement, such as a relatively slow translational speed throughout the

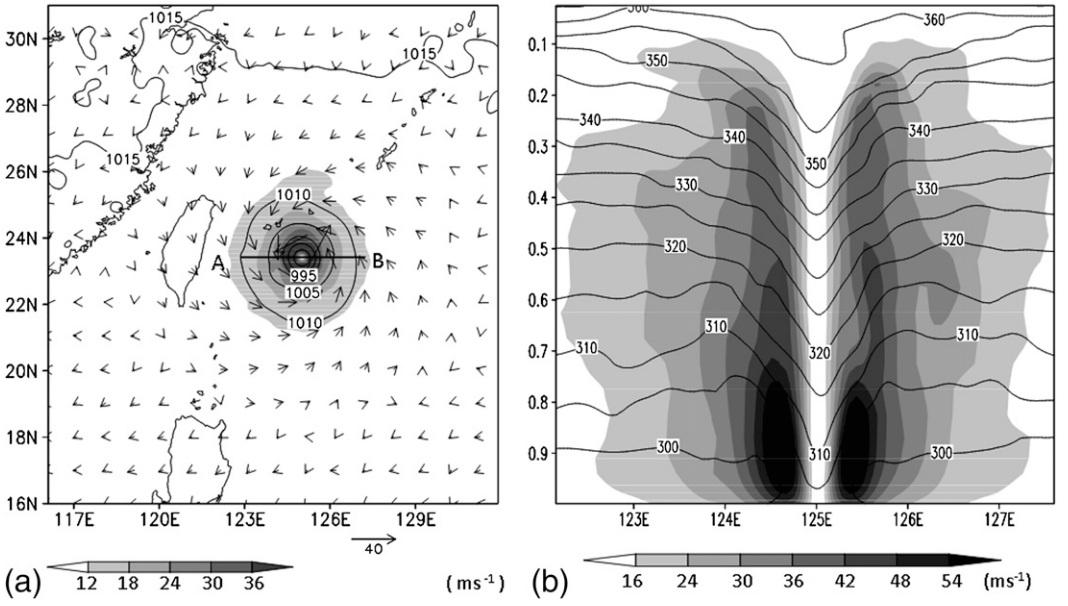

FIG. 4. As in Fig. 3, but for the initial field in idealized experiment H.

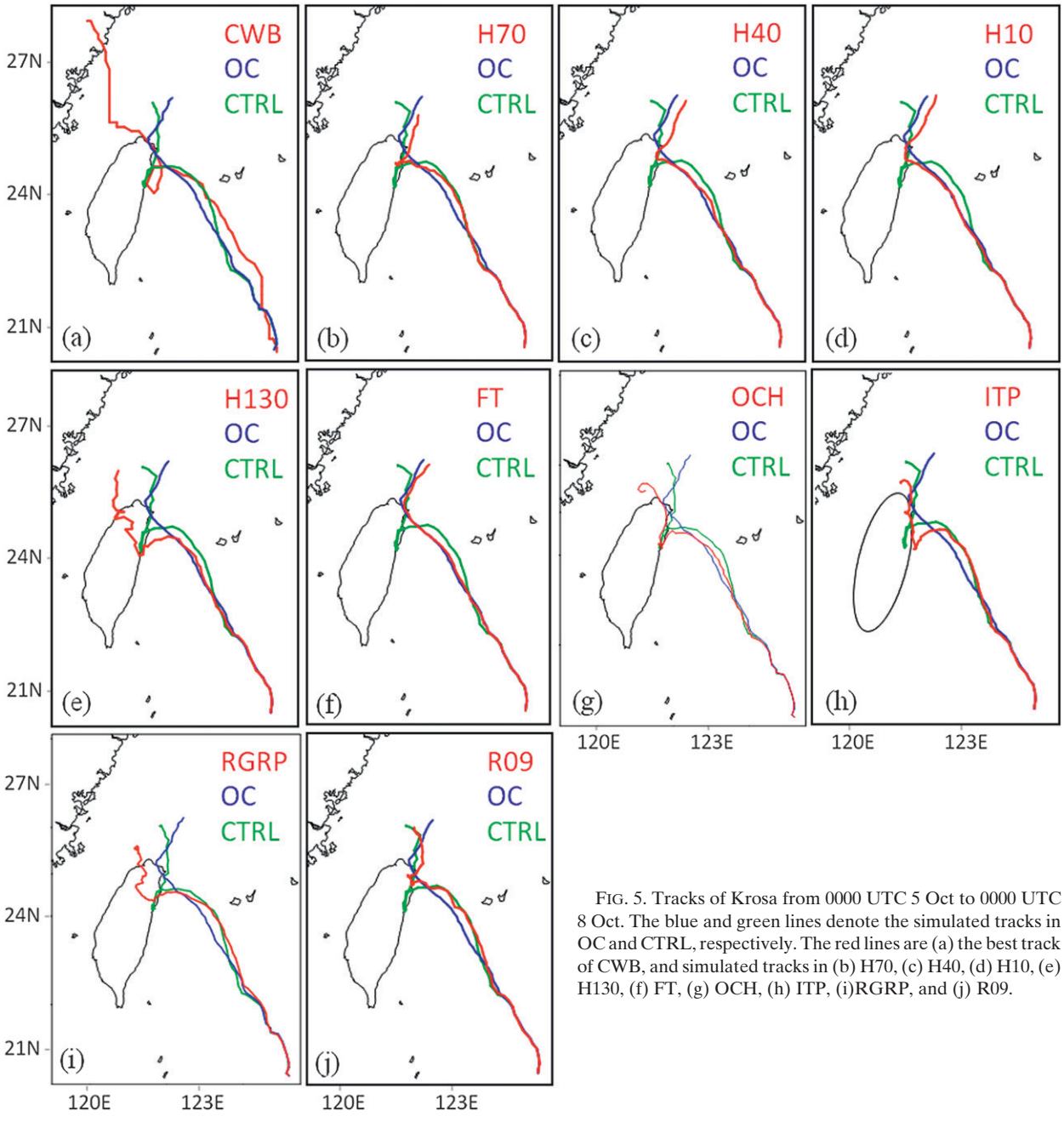

FIG. 5. Tracks of Krosa from 0000 UTC 5 Oct to 0000 UTC 8 Oct. The blue and green lines denote the simulated tracks in OC and CTRL, respectively. The red lines are (a) the best track of CWB, and simulated tracks in (b) H70, (c) H40, (d) H10, (e) H130, (f) FT, (g) OCH, (h) ITP, (i)RGRP, and (j) R09.

integration, and a track discrepancy during the later simulation hours.

The simulated Krosa in CTRL moves continuously toward the northwest during the first 38 h and then is deflected southward slightly around 39 h when the typhoon center is about 100 km from the east coast of Taiwan. Krosa heads west-northwest between 39 and 45 h of the simulation. Afterward, a dramatic southward turn occurs when the center of Krosa is about to make landfall (at around 45 h). It continuously moves southward for a distance of 50 km along the coastline from 45 to 52 h. Then, when another sharp deflection ensues at 53 h, Krosa turns to the north-northeast along the coastline, and its path is almost identical to that during the previous southward-moving episode. Although Krosa in CTRL does not make a loop, it has a kinked track, which is very similar to the looping motion in reality. This kinked track pattern can also be found in the simulated radar reflectivity (not shown). Finally Krosa leaves Taiwan at 58 h and keeps moving northwestward until the end of the simulation.

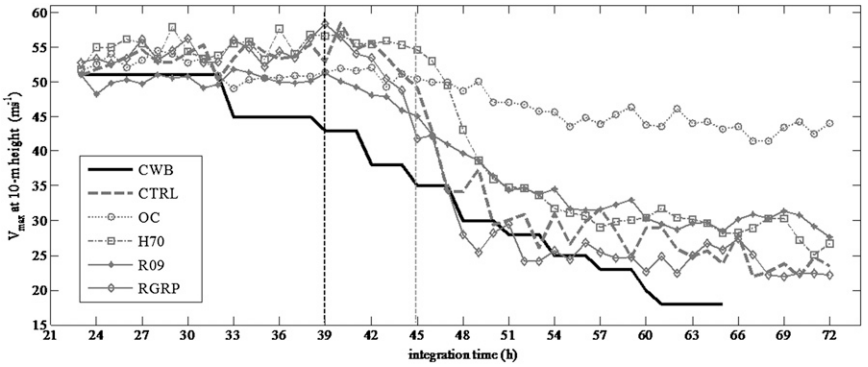

FIG. 6. Wind maximum (at 10 m) from 23 h (1 h after the finest domain is activated in the model) to 72 h (2300 UTC 5 Oct to 0000 UTC 8 Oct) in observation (CWB), CTRL, OC, H70, R09, and RGRP (see the legend). The black and gray vertical lines demonstrate the time when the storm makes landfall in observation and in CTRL, respectively.

Although CTRL captures the overall pattern of Krosa's movement during the 72-h simulation, the simulated translational speed is much slower than that observed. For example, the southward turn in CTRL is about 14 h later than observation, indicating that the simulated motion is slower than the observed before Krosa is influenced by the island's topography. Moreover, this kinked track corresponds to the looping track in the observation, but it takes 5 h longer to complete than that observed. It should be noted that the direction of the movement in CTRL is different from that in the observation during the later hours of integration. As a result of this direction deviation and the slow translational speed in CTRL, the simulated Krosa is located approximately 100 km north of Taiwan by the end of simulation, while the actual Krosa had already reached China's Fujian and Zhejiang provinces by that time. Previous studies (e.g., Chan and Gray 1982) have shown that the large-scale environmental flow dominates the majority of storm movement. It is suggested that the steering flow is not well captured in the simulation, leading to the overall slower motion and track bias during the later hours of simulation. Moreover, the difference in the simulated and actual storm structure may also have contributed to the track discrepancy in the simulation because typhoons with different structures could interact differently with the ambient flow. In spite of the track discrepancy, we believe that CTRL captures Krosa's track patterns before and during landfall, and thus can be used to investigate the mechanisms leading to the looping motion prior to Krosa's landfall.

As a result of the delayed landfall time, the storm in CTRL starts to weaken (from about 40 h) about 8 h later than that in observation (from about 32 h; Fig. 6). As shown in Fig. 6, Krosa in CTRL weakens faster than the observed; this may be due to the slower storm motion in our simulation. Besides, both CTRL and the observation show that the wind maximum starts to decrease before landfall because of the looping motion occurring near the Taiwan coast. The weakening occurs about 7 and 5 h prior to the landfall time in observation and CTRL, respectively. The terrain-induced intensity change is another important issue to be investigated in a separate study.

b. Experiment OC

In experiment OC, Taiwan topography is replaced by a flat ocean surface, and Krosa moves straight toward the northwest during the first 54 h (Figs. 1b and 5). It turns toward the northeast when its center is located at 25.23°N, 121.58°E, which is near the north coast of Taiwan. Krosa heads northeast during the remainder of the simulation. No significant southward deflection in OC occurs, in contrast to a sharp turn in CTRL. Interestingly, Krosa in experiment OC does not hit Taiwan in the simulation when the ocean condition is used to replace Taiwan topography. This result demonstrates that Taiwan's topography, rather than the environmental synoptic systems, plays the dominant role in leading to Krosa's tremendous deflection prior to and during its landfall. Our main interest is to understand how Taiwan's topography causes Krosa's looping motion. This will be addressed with advanced analyses in the following sections.

The significant track difference between CTRL and OC simulations before or after the large southward turn occurs is also worthy of investigation. Under the influence of topography, the typhoon in CTRL is slightly deflected to the left of the OC track from 17 to 20 h when Krosa is around 300–350 km from the island. As Krosa is approaching the topography, the direction of the track deflection in CTRL alters and becomes more prominent. Krosa in CTRL starts to be deflected to the right of the OC track after 21 h of simulation when its

center is about 250 km east of the coast and then moved cyclonically before making landfall. The cyclonic movement starts north-northwestward and then toward the northwest and west when the typhoon center is about 100 km upstream of Taiwan's topography. After that, a sharp southward turn occurs in CTRL when the typhoon center is about to make landfall. Different from that in CTRL, the typhoon in OC keeps heading northwestward in a straight path during the same time period. Comparing the tracks in CTRL and OC, it is shown that Krosa's motion is initially influenced by the orography when its center is around 350 km upstream of Taiwan's topography. This impact distance from the Taiwan topography is consistent with the results of Yeh and Elsberry (1993a), in which a vortex starts to be deflected when located between 250 and 400 km upstream (their region B) heading toward a terrain barrier.

After Krosa leaves Taiwan topography, the tracks in OC and CTRL are different as well. Krosa heads northward in CTRL, while it moves toward the northeast in OC. This suggests that topography not only influences the movement upstream, but also lead to distinct track deviation downstream. The impact of topography on tracks downstream can be due to terrain-induced environmental flow variations, vortex structure changes (e.g., asymmetric flow), and intensity change. This is an interesting topic for future study since the focus of present study is on Krosa's sharp southward turn prior to its landfall.

c. *Influence of the terrain height*

Since the presence of the Taiwan topography is shown to be responsible for the significant track deflection of Krosa prior to its landfall, it is interesting to explore which aspects of the terrain have a dominant impact on the typhoon's track and which mechanism is involved. These include the terrain height, surface properties (e.g., land or ocean), and details in topographic 3D shape. Since terrain height is likely to contribute to track deflection, we conduct five experiments by varying the Taiwan terrain height: FT, H10, H40, H70, and H130. The terrain heights of these experiments are reduced to 0%, 10%, 40%, 70%, and increased to 130% of that in CTRL, respectively. Aside from the terrain height over Taiwan, all other settings are identical to those in CTRL.

The results demonstrate that the magnitude of the deflection prior to landfall is reduced when the terrain height is lowered (Fig. 5), in agreement with the findings in Jian and Wu (2008). While a cyclonic track prior to landfall similar to that in CTRL shows in H70 (Fig. 5b), no southward turn occurs, in contrast to that in CTRL. Only a westward path takes place as Krosa is about to make landfall in H70. After Krosa leaves Taiwan, the track in H70 is slightly to the east of that in CTRL, and becomes more similar to that in OC. As the terrain height is reduced to 40% and 10% of that in CTRL (H40 and H10), the movement of Krosa is quite similar to that in OC (Figs. 5c,d). Eventually, there are only small differences between OC and FT (Fig. 5f). In H130, a simulation with higher topography than that in CTRL, the storm is deflected earlier; a kinked track also occurs near the topography, similar to that in CTRL. These results demonstrate that it is the Taiwan terrain height that leads to the major deflection of Krosa prior to its landfall. The small difference in the track between OC and FT implies that the surface properties appear to play little role in deflecting Krosa; this will be further verified in OCH in section 4d.

d. *Sensitivity to surface properties and details in terrain shape*

The effect of surface properties on Krosa's movement has already been seen from the simulated tracks in FT, OC, and CTRL. This is further verified in another experiment OCH, in which the land surface in CTRL is replaced by ocean. Namely, OCH is a simulation with the Taiwan topography covered by a water surface, which serves as an obstacle, but provides surface latent heat flux similar to that in OC and less friction than that in CTRL. The resultant track is almost identical to that in CTRL, while distinctly different from that in OC (Fig. 5g). This further demonstrates that the surface properties play a second role in deflecting Krosa. Even though the ocean surface can provide latent heat continuously, the elevated topography can influence Krosa's movement greatly, leading to the significant track deflection.

Experiment ITP (Fig. 5h) with an idealized topography (Fig. 7d) almost duplicates the track pattern in CTRL, implying that complicated topographic shapes of CMR play a trivial role in varying Krosa's movement. Additionally, the result of ITP also indicates that the use of this idealized orography to study TC track deflection induced by Taiwan-like topography is appropriate; at least for typhoons approaching northern Taiwan (such as Krosa). For this reason, this idealized topography is utilized in the idealized experiments as discussed in the next section.

e. *Sensitivity to model resolution and cloud microphysics*

R09, a simulation with coarser model horizontal resolution (9 km), does not capture the track deflection well during Krosa's landfall (Fig. 5j). Different from CTRL, R09 does not turn significantly southward during its landfall; it deflects to the north-northwest right after the landfall and turns to the northeast when leaving the

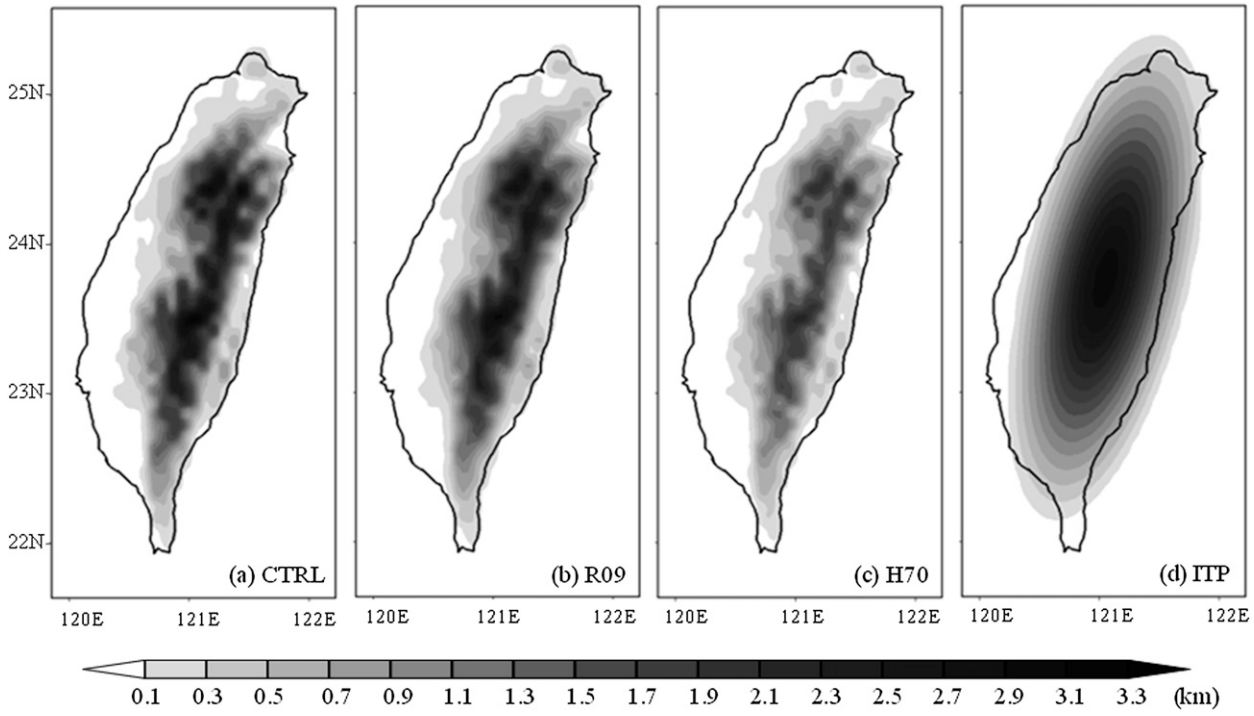

FIG. 7. The model terrain height in (a) CTRL, (b) R09, (c) H70, and (d) ITP.

Taiwan topography. R09 has a cyclonic movement until the end of the simulation. Despite the difference in tracks between CTRL and R09 during the landfall, the typhoon center in R09 is close to that in CTRL at the end of the integration. Actually, the movement near the topography in R09 appears similar to that in H70, and shows no significant kinked track during the landfall. The result of R09 implies that the model resolution is important in studying this unusual sharp track deflection induced by high terrain. The differences between the tracks of R09 and CTRL may be due to the reduced model terrain height, or the vortex structure, the vortex intensity, or the topography–typhoon interaction (such as the channeling flow, etc.) in different model resolutions. To identify the value of the model resolution, first, the model topography in CTRL, R09, and H70 is examined. We find that the terrain height and its distribution in R09 (Fig. 7b) are similar to those in CTRL (Fig. 7a), while they are quite different from those in H70 (Fig. 7c). This indicates that the differences between the tracks in CTRL and R09 are not due to the variations of the terrain height constructed by two different model resolutions. Therefore, the key impacts of the model resolution on tracks can only be related to variations in vortex intensity, structure, or the terrain–vortex interaction. After the third domain is initiated, the vortex in CTRL intensifies, but the vortex in R09, without the third domain, does not. As shown in Fig. 6, the maximum wind in R09 is about 4.5 m s^{-1} weaker than that in CTRL before the southward deflection begins (around 39 h). The structure change further shows that the wind speed increase between Krosa and the topography is much weaker and is only present for 2–3 h in R09 (figures not shown) prior to and during landfall. Hence, the vortex is not significantly deflected southward. The small enhanced wind at the channel in R09 is probably related to its weaker intensity. The barrier-induced intensity dissipation is likely more significant than the wind enhancement due to the channeling effect.

To address concerns that the microphysics scheme adopted in our simulation might affect the results, sensitivity tests are performed to clarify the influence of the microphysics scheme on typhoon track, particularly on that prior to landfall. In RGRP, an experiment with a more complicated cloud microphysics scheme (Reisner 2), the track is not significantly affected before landfall compared with that in CTRL. However, the deviations occur after Krosa makes landfall (Fig. 5i). Krosa in RGRP is deflected less northward than in CTRL and thus crosses northern Taiwan, while it detours Taiwan in CTRL and in the best track. Note that the result does not imply that the simple ice cloud microphysics scheme used in CTRL is more adequate for typhoon simulation. Rather it demonstrates that the track deflection could depend on the cloud microphysical processes to some degree, in particular when Krosa is crossing the

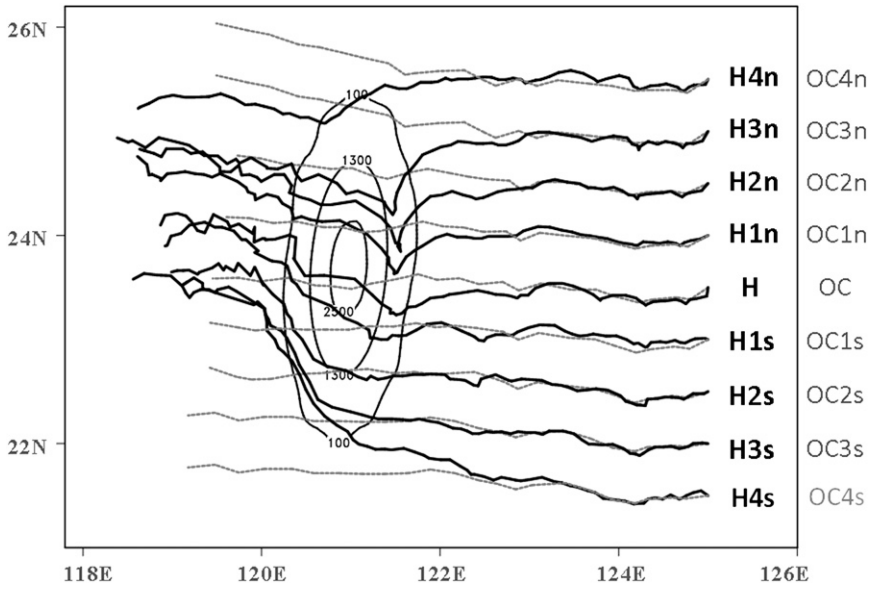

FIG. 8. Tracks simulated in the idealized experiments. Gray dashed lines are simulations with no topography (OC group), while the black solid lines are those with topography (H group.) Black contours marked with numbers (100, 1300, 2500) indicate the terrain height (m). The *x* and *y* axis are longitude and latitude, respectively. The names of each experiment are listed on the right side of the figure, with corresponding shading to that of their tracks.

topography. In addition, a lot of studies have indicated the important role of model cloud microphysics in the terrain-induced typhoon intensity change (e.g., Wu et al. 2003a, 2009a) and the associated precipitation (e.g., Wu et al. 2002, 2009b). Intensity evolution in CTRL and RGRP (Fig. 6) shows differences during the postlandfall period (48–63 h), but the differences are not significant except at 48 and 49 h. Accordingly, we suggest that the current study using the simple ice scheme can reasonably assess the topography–typhoon interactions, especially prior to landfall and during early landfall periods. Although these issues are beyond the scope of our current study, they are important in typhoon forecast and need to be studied further in the future.

5. Results of the idealized experiments

The results from the simulations of Krosa discussed in section 4 suggest that Krosa would not have made landfall in Taiwan if the island topography were not lofty. This leads to an interesting hypothesis that the Taiwan's topography is likely to attract the typhoons that pass by the ocean north to Taiwan. To evaluate the distance at which the topography affects storm tracks, as well as the terrain-induced track variations for vortices approaching different parts of the topography, a series of idealized experiments are introduced in this section.

The storm in "OC" group shows consistent behaviors in the movement (Fig. 8). The westward motions show small fluctuations during the early stage and then become straight and smooth during the rest of the integration. In H group (Fig. 8), prominent track deflection occurs under the influence of topography. Southward deflection is found when the vortex approaches the northern and the central part of the topography. These vortices (H4n, H3n, H2n, H1n, and H) start to veer southward when they are around 150 km east of the topography. Moreover, vortices approaching the northern tip of the topography (H3n and H2n) are deflected more southward than those approaching the central topography (H1n and H.) However, when the vortex is located too far north to the topography (H4n), the southward deflection will be greatly reduced. After making landfall, the vortices, with eminent southward deflection, turn sharply to the northwest, displaying a kinked track.

In contrast, vortices approaching the southern part of the topography (H1s, H2s, and H3s) show much less deflection prior to landfall. Unlike other vortices approaching the southern part of the topography, the vortex located to the southeast (H4s) is initially deflected to the north when it is about ~100–150 km east of the topography. After landfall, the vortices approaching the southern part of the topography, namely, H1s, H2s, H3s, and H4s, are deflected to the north significantly. The more to the south the vortex is located; the more it is deflected to the

north. However, this kind of northward deflection, which occurs when a typhoon is leaving the topography, has not been observed based on the CWB typhoon database. It is notable that the tracks in our idealized experiments are different from those simulated by Yeh and Elsberry (1993a) in their much coarse resolution (45 km) model with weaker vortices and lower terrain height. As shown in Yeh and Elsberry (1993a), vortices approaching different parts of the topography are all deflected northward prior to landfall (see their Fig. 12), while the deflection is less evident for the more intense vortices (see their Fig. 21). In contrast, intense vortices in this study can be significantly deflected by the topography, especially prior to and during their landfall. More detailed discussions and comparisons between the simulations in Yeh and Elsberry (1993a) and those in this research are presented in the final section.

6. Typhoon–terrain interaction

We will introduce wind and trajectory analyses in this section to provide further insight into the mechanism involved in typhoon–terrain interactions, which cause track deflection. Examining the low-level wind field from the 1-h model output, we find that strong low-level winds appear in a channel between the storm and the topography and are enhanced (e.g., Fig. 9) when a large deflection occurs to the typhoon in CTRL. Consequently, the strong winds are likely to form a northerly jet, which may steer Krosa southward. On the contrary, there is no obvious wind increase in OC (Fig. 10). Similar wind enhancement is evident over the channel in the idealized experiments with significant deflected motion near the topography (e.g., H3n shown in Figs. 11, 12 and H3s shown in Fig. 13). However, winds to the west of vortex's center do not strengthen in OC of Krosa and in the OC group of the idealized experiments during the same time period (Figs. 10 and 14), indicating that the typhoon–terrain interaction is the key to the channel wind development and the southward deflection of an intense typhoon.

Meanwhile, the backward-trajectory calculations of the low-level air parcels show the confluent trajectories when the air column passes through the channel between the high terrain and the typhoon vortex during the southward deflection period in CTRL (Figs. 9a,b). Air parcels at higher levels do not converge when passing the channel between the terrain and storm (Figs. 9c,d). This result is consistent with the concept of channeling effect (e.g., Lin et al. 1999, 2005; Jian and Wu 2008). Consistent results are found in the idealized experiments. The low-level confluent trajectories in the inner-core region show the occurrence of the channeling effect when the vortex is deflected to the south in H, H1n, H2n (figures not shown), and H3n (Figs. 11a and 12a,b). The confluent trajectories over the channel between the barrier and storm are also found in vortices leaving the topography with significant northward deflection (e.g., H3s, shown in Fig. 13). In contrast, the channeling effect occurs in neither OC of Krosa (Fig. 10) nor the OC group of idealized simulations (Fig. 14) because the trajectories in those experiments are parallel during the same period, implying that the confluent trajectories are induced by the topography. Consistent results in Krosa simulations and idealized experiments indicate that the *channeling effect* plays an important role in inducing the strong winds in the channel between the high topography and the storm and thus the southward turning of the storm prior to landfall, in agreement with the conceptual pictures of Lin et al. (2005) and the findings of Jian and Wu (2008).

Following Jian and Wu (2008), the asymmetric flow in the inner-core region (within 100-km radius) and the storm motion are compared to understand the relationship between the winds induced by the channeling effect and the great southward deflection. The evolution of the asymmetric flow in the inner-core region and the storm motion have a similar trend in both CTRL (Fig. 15) and OC (Fig. 16). Calculations in the inner-core region within 50-km radius show similar results (figures not shown). Northerly asymmetric flow is absent in OC but present in CTRL when the CTRL storm is deflected southward, indicating that the asymmetric flow in the inner-core region likely contributes to changes in the typhoon movement. However, the asymmetric flow does not match Krosa's motion vector perfectly. This is different from that found in Typhoon Haitang (Jian and Wu 2008). The difference may be due to the essential deviation in the location where the looping motion took place. The southward turn of Krosa occurred over the east coast of Taiwan, while Haitang made a loop over the ocean in the simulation of Jian and Wu (2008). Krosa is influenced by the mesoscale topographic features much more significantly (Fig. 7), so that it shows much finer structure during the period of looping motion (figures not shown). The asymmetric flow over Krosa might be largely affected by small-scale motions and is not well defined when it is located in the vicinity of the topography compared with that over Haitang. Therefore the asymmetric flow over the storm core, often referred to as the steering flow, would not be expected to explain the typhoon motion as the only contributing factor. Despite the fact that the asymmetric flow in the inner-core region could not match Krosa's looping motion perfectly, the inner-core asymmetric winds undoubtedly contribute greatly to the sharp southward turning motion of Krosa in CTRL.

As shown in Lin et al. (2005), some vortices are deflected southward prior to landfall under certain flow

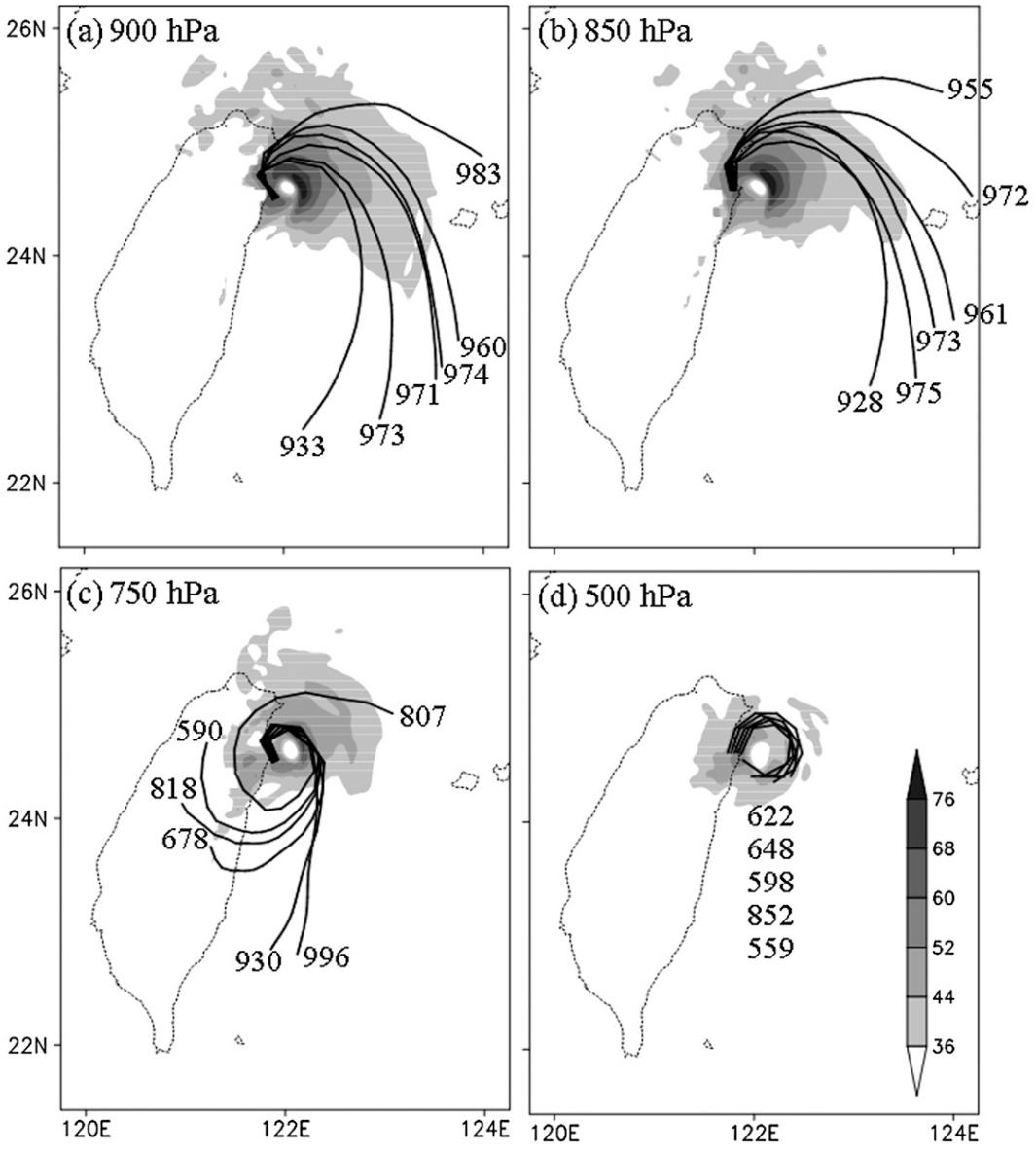

FIG. 9. Backward trajectories based on the simulated winds from experiment CTRL. Parcels are released at (a) 900-, (b) 850-, (c) 750-, and (d) 500-hPa pressure levels at 43 h and calculated backward for 3 h in (a), (b), and (c), and for 2 h in (d). Horizontal wind speeds at 43 h are shaded for values greater than 36 m s^{-1} (as shown in the grayscale). Numbers beside each trajectory are the pressure level (hPa) of the parcel at the end of the backward trajectories.

regimes (see their Fig. 5). To understand the flow regimes favoring the southward track deflection in the simulations with more realistic settings, the six nondimensional parameters suggested by Lin et al. (2005) are calculated in our idealized experiments. Above the boundary layer, the Froude numbers of the vortex and the basic flow are around 2–3 and 0.15–3, respectively. The Rossby numbers of the vortex and the basic flow are approximately 6.5 and 0.55, respectively. The steepness of the topography is 0.02 and the ratio of the vortex size to the scale of topography is 0.625. Compared with the Table 2 of Lin et al. (2005), the Froude number and Rossby number of the vortex are large while those of the basic flow are small. This is relevant to the more intense vortices and the moderate speed of the basic flow in our simulations. Values of the six parameters in our simulations do not fit any cases in Lin et al. (2005.) The most similar simulation may be F6, which is also a case with southward track deflection. However, the Rossby number of the vortex and the steepness of topography are quite different. That is to say, the flow regimes in our simulations were not investigated by Lin et al. (2005).

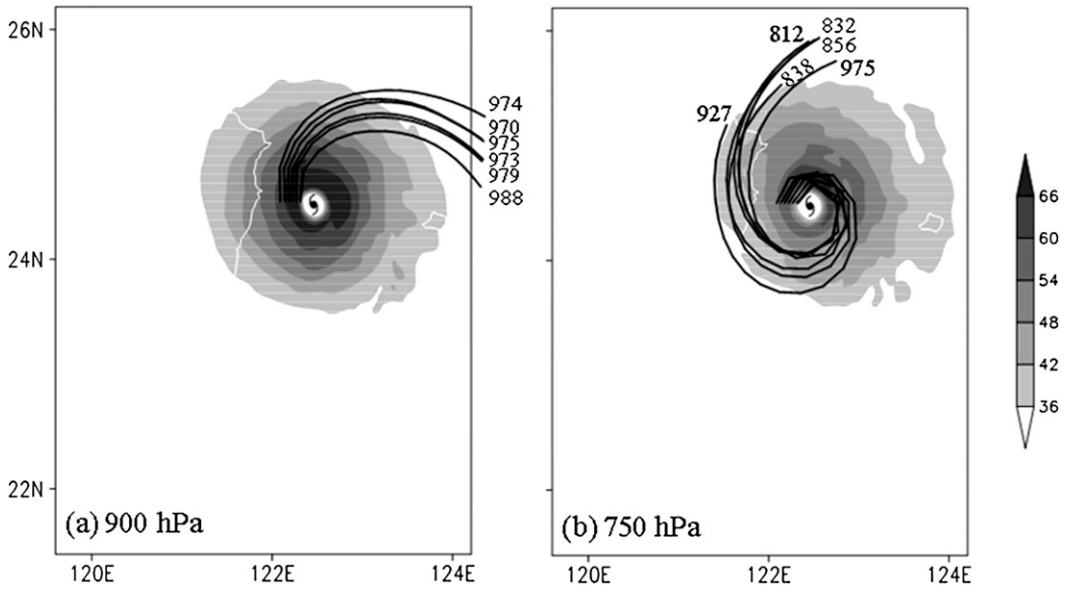

FIG. 10. Backward trajectories based on the simulated winds from experiment OC. Parcels are released at (a) 900- and (b) 750-hPa pressure levels at 39 h and calculated backward for 3 h. Horizontal wind speeds at 39 h are shaded for values greater than 36 m s^{-1} (as shown in the grayscale). Numbers beside each trajectory are the pressure levels (hPa) of the parcel at the end of the backward trajectories.

Moreover, vortices with different initial latitudinal positions have identical values of these six parameters. However, their movements near the topography can be greatly different. It is clear that the flow regimes leading to the southward track deflection prior to landfall should be further studied and should include more parameters, in particular parameters related to the initial latitudinal position of the vortex or the portion of the topography that the typhoon vortex is approaching.

7. Conclusions and discussion

In this study, the eminent deflection of typhoon track prior to its landfall over the mountainous island

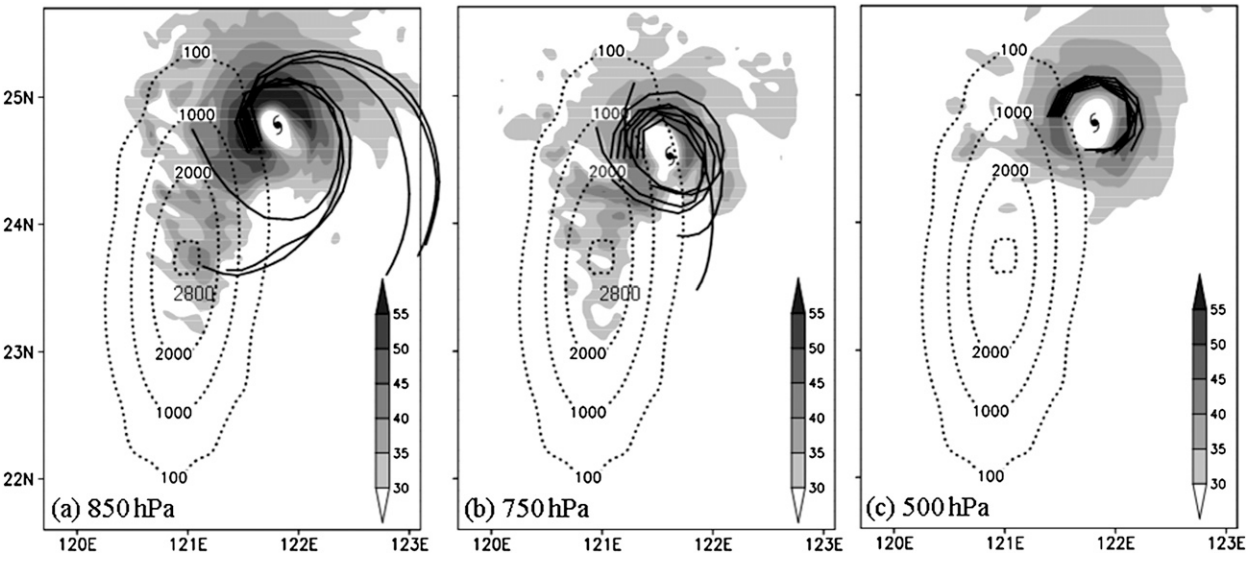

FIG. 11. Backward trajectories based on the simulated winds from experiment H3n. Parcels are released at (a) 850-, (b) 750- and (c) 500-hPa pressure levels at 37 h and calculated backward for 3 h in (a) and for 1 h in (b) and (c). Horizontal wind speeds are shaded for values greater than 30 m s^{-1} (as shown in the grayscale).

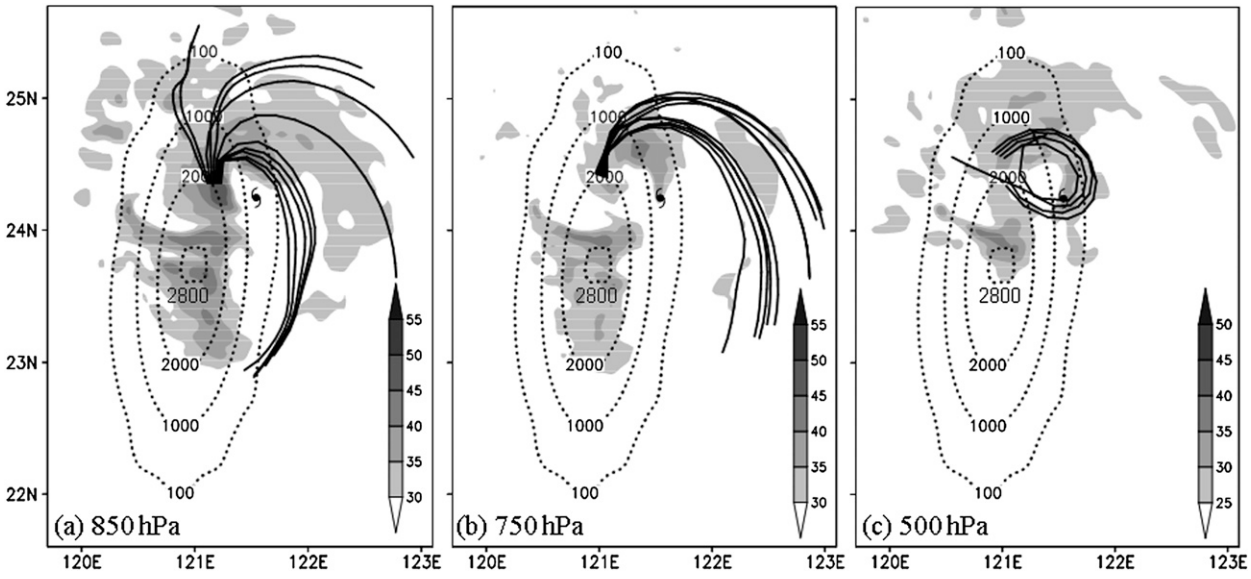

FIG. 12. As in Fig. 11, but the parcels being released at 43 h and calculated backward for 3h in (a) and (b) and for 2h in (c).

topography of Taiwan is studied based on high-resolution simulations for Typhoon Krosa (2007) and a set of idealized experiments using a full-physics model. Results from both the real-case simulations of Krosa and the idealized experiments demonstrate that the high topography plays an important role in the TC track deflection, consistent with many previous studies (e.g., Bender et al. 1987; Yeh and Elsberry 1993a; Lin et al. 1999, 2005; Jian and Wu 2008). The significant southward deflections over the northern and central Taiwan in our idealized simulations have been found in the historically observed cases (e.g., those with looping motion) prior to landfall, while this unique track deflection has not been investigated comprehensively in previous numerical studies. We show that the terrain height of Taiwan plays the most important role in Typhoon Krosa's looping motion at its landfall while the surface properties, details in the topographic shape, and the cloud microphysics impose much

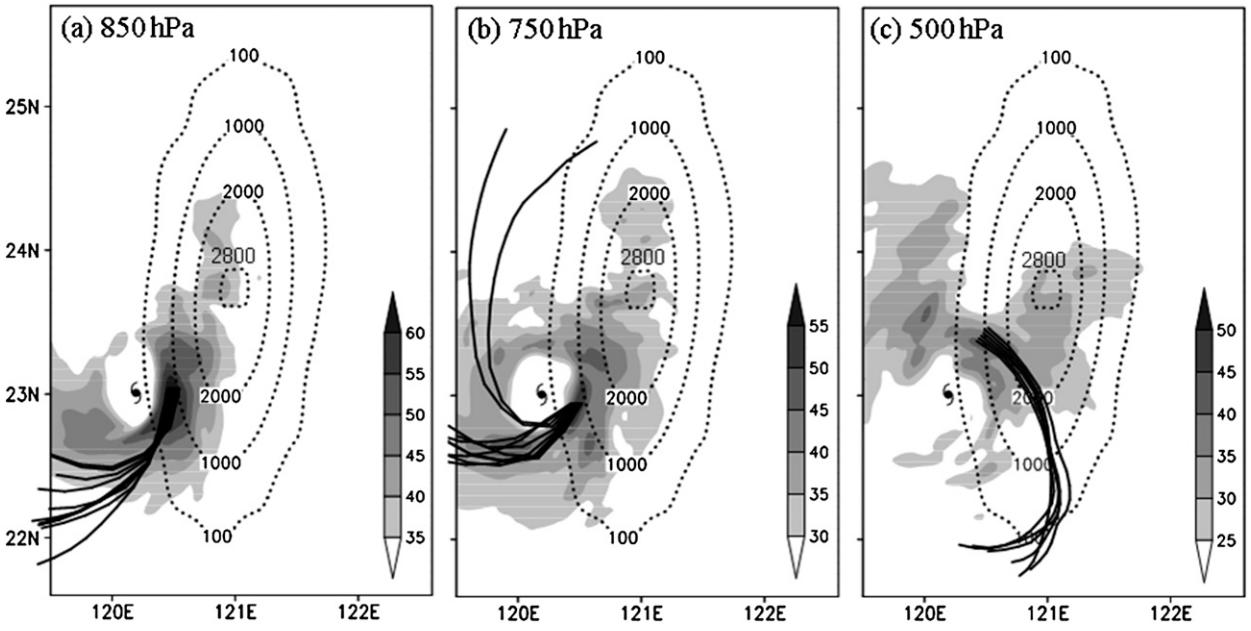

FIG. 13. As in Fig. 12, but for experiment H3s. Parcels are released at (a) 850-, (b) 750-, and (c) 500-hPa pressure levels at 56 h and calculated backward for 3 h.

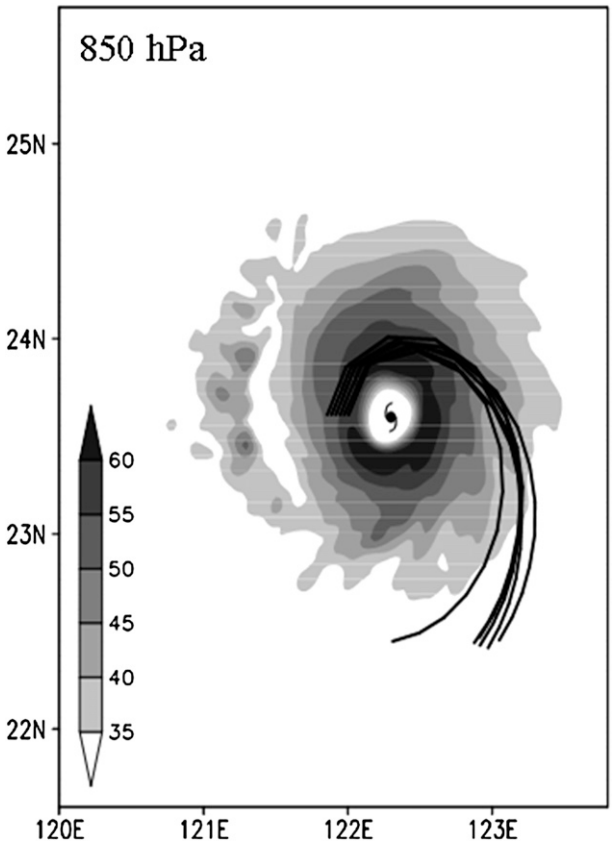

FIG. 14. Backward trajectories based on the simulated winds from the idealized experiment OC. Parcels are released at 850-hPa pressure levels at 34 h and calculated backward for 3 h. Horizontal wind speeds at 34 h are shaded for values greater than 35 m s^{-1} (as shown in the grayscale).

weaker impacts on the track. Results from idealized simulations show that vortices near the northern and central parts of the topography are significantly deflected to the south prior to landfall and during the incipient landfall period. Then they turn sharply to the north forming a kinked track pattern, which is similar to the observed looping cases in Taiwan. For vortices over the central and southern portions of the topography, they are deflected northward when leaving the topography. Furthermore, simulations with a high resolution (3 km) and realistic model settings reproduce the observed Krosa's track, while that with a coarser resolution (9 km) fails, indicating that high resolution is important for the prediction and simulation of the terrain-induced typhoon track deflection. Analyses show that the intensity and its evolution in CTRL and R09 (Fig. 6) are different. The wind maximum is about 5 m s^{-1} stronger in CTRL before landfall. The intensity difference may lead to variations in movement because vortices are steered by environmental flows of different depths. However, the tracks in CTRL and R09 are nearly the same before the significant southward sharp turn occurs in CTRL, suggesting that the difference in the depth of steering flow may not be the key factor for the track variation prior to landfall. Topographic influences on storms may vary with different intensities as well. The intensification prior to landfall and the rapid weakening in CTRL (Fig. 6) support this speculation and suggest that finer resolution (3 km) can help capture more eminent topographic influences. No significant wind is enhanced over the channel between the vortex center and the terrain prior to landfall in R09 (figures not shown). Based on the above discussions, we infer that the differences in intensity and terrain-induced structure change performed by 3- and 9-km resolutions would likely lead to the variations in the terrain-induced deflection.

Both real-case and idealized simulations show strong channel winds enhanced between the storm and the terrain when a southward deflection occurs. The backward trajectory analyses further support the concept of channeling effect, which is found to be crucial to deflect Typhoon Haitang (2005) southward in Jian and Wu (2008). Evolution of the inner-core asymmetric flow and storm motion does show that the sharp southward and northward turns before and after the landfall can be mainly attributed to the asymmetric flow (Fig. 15). The northerly flow enhanced by the channeling effect is likely to deflect the storm southward, while the southerly flow due to the terrain-induced weakening to the west of the storm may deflect the storm northward. This suggests that the track deflection prior to landfall results mainly from the significant terrain-induced asymmetric vortex structure. In addition, the results also show that the inner-core asymmetric ventilation flow, however, does not match the movement of a deflected typhoon perfectly, partly because the asymmetric flow is not well defined and could not completely capture the terrain-induced deflection in the simulation and in nature.

Note that the vortex movements prior to landfall in our idealized simulations do not agree well with those shown by Yeh and Elsberry (1993a), in which a much coarse-resolution (45 km) model was used, and weaker vortices and lower terrain height were implanted. In this study, vortices with intensity of a supertyphoon approaching the northern and central topography are deflected significantly southward, while those approaching the southern part are barely deflected or deflected to the north. In contrast, all vortices in Yeh and Elsberry (1993a)'s experiments were deflected northward prior to landfall (their region C), while the deflection was insignificant in the simulations with stronger (but still weak compared to those in our study) vortices. Yeh and Elsberry (1993a), Jian and Wu (2008), and the analyses in this study all suggest that the presence of topography

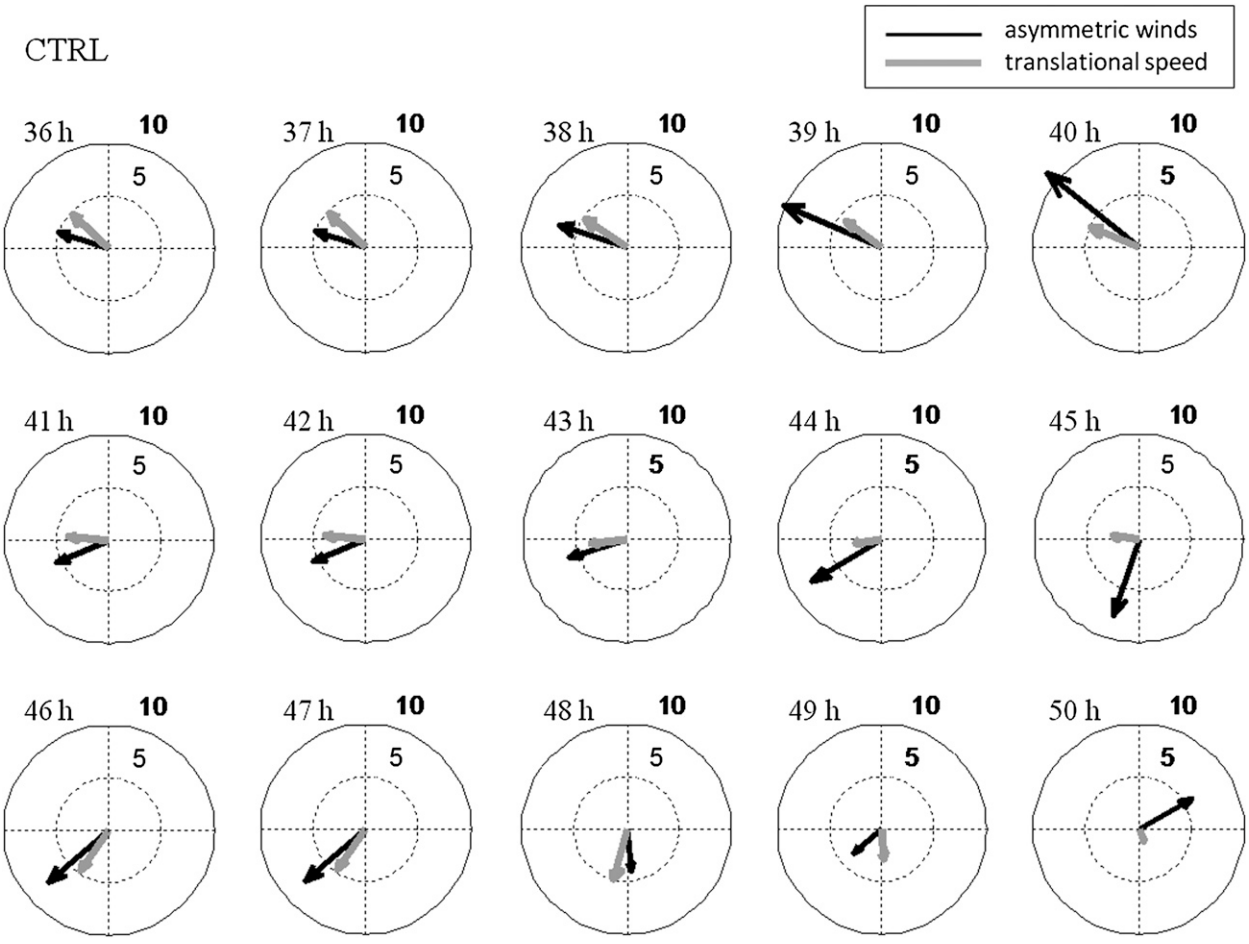

FIG. 15. Deep-layer mean of area-averaged asymmetric wind (σ = 0.9775–0.175) within 100-km radius (black) and translational speed (gray) in CTRL. Inner and outer circles indicate the magnitude of 5 and 10 m s^{-1}, respectively.

can induce inner-core asymmetric flow to deflect a typhoon significantly near the topography. These studies all demonstrate that the asymmetric flow leading to the northward track deflection is attributed to the further weakening of flows between the storm center and topography due to the destruction of topography. However, the distances from the topography at which the southerly asymmetric flow or the northward deflection appears are different. The northward deflection was present within 250 km upstream of the terrain in Yeh and Elsberry (1993a), while it occurs within around 60 km upstream of the topography in Jian and Wu (2008) or after landfall in the simulations in this study (i.e., CTRL and the H group experiments). As to the southward track deflection, Yeh and Elsberry (1993a), Lin et al. (1999, 2005), Jian and Wu (2008), and this study all suggest that the channeling effect is likely to play a dominant role. However, Yeh and Elsberry (1993a) attributed the southward deflection in their region B to the enhancement of the storm's outer circulation over the channel. Both Jian and Wu (2008) and this study demonstrate the key role of the significant inner-core wind increase induced by the channeling effect just prior to the landfall and during the incipient landfall period. In addition, the simulations in this study show that the topography can have great impact on the movement of an intense typhoon. This typhoon–terrain interaction has not been depicted in earlier idealized numerical studies with much coarser model resolutions. This implies that the interaction between an intense typhoon and high terrain is a very important issue and can only be realistically captured in the simulations with fine resolutions. In the meantime, the flow regimes in our simulations are beyond the parameter space investigated by Lin et al. (2005). Therefore, the flow regimes leading to the southward track deflection prior to landfall should be further studied with the parameter space refined, in particular, to include parameters related to the initial latitudinal position of the vortex or the portion of the topography the typhoon vortex is approaching.

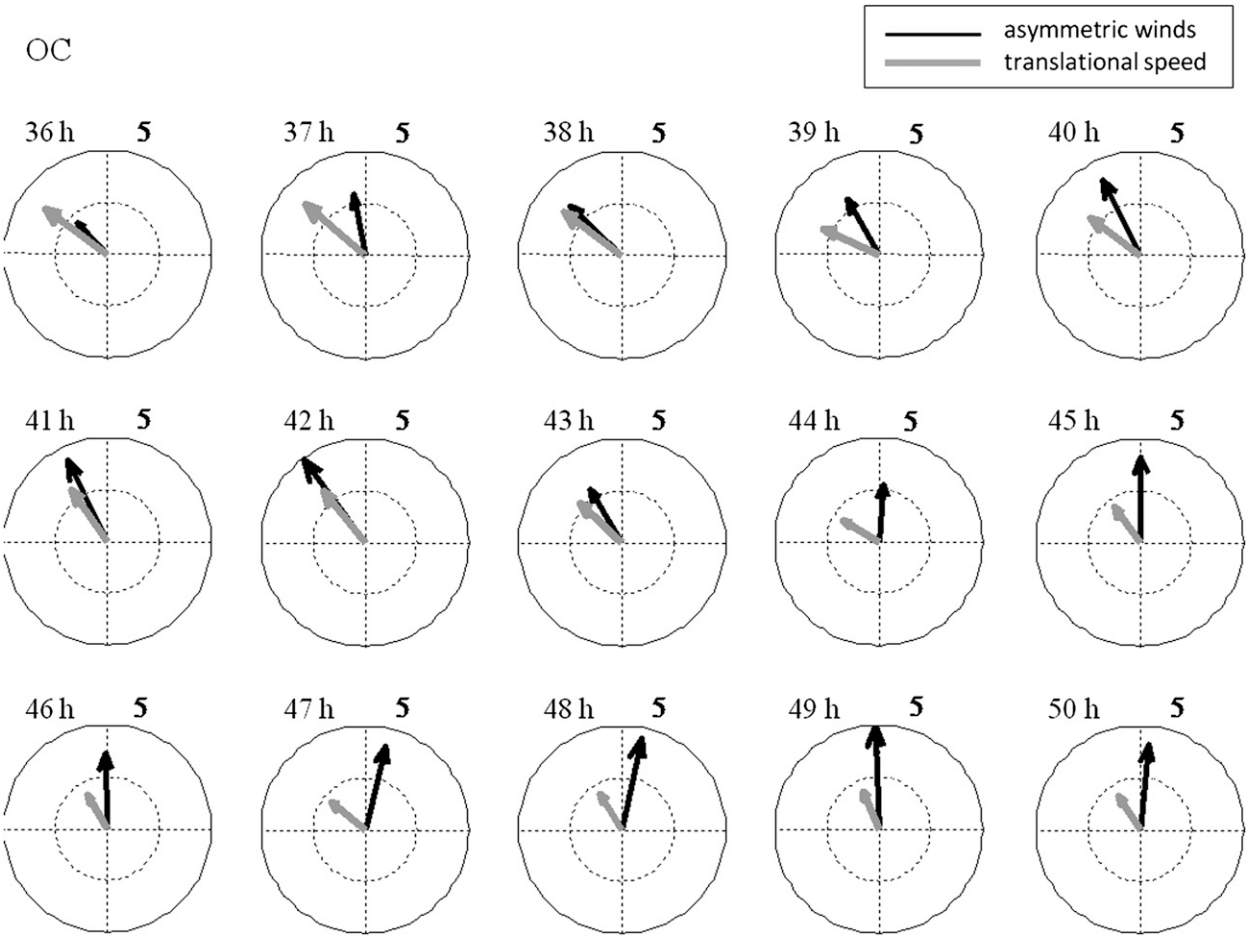

FIG. 16. As in Fig. 15, but for OC. Inner and outer circles indicate the magnitude of 2.5 and 5 m s^{-1}, respectively.

Finally, although our analyses demonstrate the important role of the channeling effect in leading to the sharp southward track deflection prior to landfall, the channeling effect could depend considerably on the intensity and structure of the typhoon itself, the magnitude of the ambient flow, and the impinging angle. These are topics of our ongoing research for which carefully designed experiments are to be carried out to identify the flow regimes leading to specific track deflections. We expect that a full investigation on terrain-induced track deflection will further shed light on the terrain-induced changes in typhoon strength and structure, and most importantly the associated rainfall distribution.

Acknowledgments. This work is supported by the National Science Council of Taiwan Grant NSC 98-2111–M-002-008–MY3. Yuqing Wang is partly supported by NSF Grant ATM-0754039. We appreciate Treng-Shi Huang for providing the idealized settings to construct the initial field in MM5. We also thank Guo-Ji Jian, Ching-Yuang Huang, Ming-Jen Yang, and Cheng-Ku Yu for their helpful comments. Valuable comments from two anonymous reviewers are also greatly appreciated.

REFERENCES

Bender, M. A., R. E. Tuleya, and Y. Kurihara, 1987: A numerical study of the effect of island terrain on tropical cyclones. *Mon. Wea. Rev.,* **115,** 130–155.

Blackadar, A. K., 1976: Modeling the nocturnal boundary layer. Preprints, *Third Symp. on Atmospheric Turbulence and Air Quality,* Raleigh, NC, Amer. Meteor. Soc., 46–49.

——, 1979: High resolution models of the planetary boundary layer. *Advances in Environmental and Scientific Engineering,* J. Pfafflin and E. Ziegler, Eds., Vol. I, Gordon and Breach, 50–85.

Brand, S., and J. W. Blelloch, 1974: Changes in the characteristics of typhoons crossing the island of Taiwan. *Mon. Wea. Rev.,* **102,** 708–713.

Chan, J. C. L., and W. M. Gray, 1982: Tropical cyclone movement and surrounding flow relationship. *Mon. Wea. Rev.,* **110,** 1354–1376.

Chang, S.-W., 1982: The orographic effects induced by an island mountain range on propagating tropical cyclones. *Mon. Wea. Rev.,* **110,** 1255–1270.

Charney, J., 1955: The use of primitive equations of motion in numerical prediction. *Tellus,* **7,** 22–26.

DeMaria, M., and J. C. L. Chan, 1984: Comments on ''A numerical study of the interactions between two tropical cyclones.'' *Mon. Wea. Rev.,* **112,** 1643–1645.

Dudhia, J., 1989: Numerical study of convection observed during the winter monsoon experiment using a mesoscale two-dimensional model. *J. Amots. Sci.,* **46,** 3077–3107.

Grell, G. A., J. Dudhia, and D. R. Stauffer, 1995: A description of the fifth-generation Penn State/NCAR Mesoscale Model (MM5). NCAR Tech. Note NCAR/TN-398STR, 122 pp.

Huang, T.-S., M. Montgomery, and C.-C. Wu, 2008: Sensitivities of hurricane intensity to planetary boundary layer schemes in a full physics three dimensional nonhydrostatic mesoscale model. Preprints, *28th Conf. on Hurricanes and Tropical Meteorology,* Orlando, FL, Amer. Meteor. Soc., 3A.5. [Available online at http://ams.confex.com/ams/28Hurricanes/techprogram/paper_137768.htm.]

Jian, G.-J., and C.-C. Wu, 2008: A numerical study of the track deflection of Super-Typhoon Haitang (2005) prior to its landfall in Taiwan. *Mon. Wea. Rev.,* **136,** 598–615.

Jordan, C. L., 1958: Mean soundings for the West Indies area. *J. Meteor.,* **15,** 91–97.

Lin, Y.-L., J. Han, D. W. Hamilton, and C.-Y. Huang, 1999: Orographic influence on a drifting cyclone. *J. Atmos. Sci.,* **56,** 534–562.

——, S.-Y. Chen, C. M. Hill, and C.-Y. Huang, 2005: Control parameters for the influence of a mesoscale mountain range on cyclone track continuity and deflection. *J. Atmos. Sci.,* **62,** 1849–1866.

Smith, R. B., 1989: Comment on ''Low Froude number flow past three-dimensional obstacles. Part I: Baroclinically generated lee vortices.'' *J. Atmos. Sci.,* **46,** 3611–3613.

Smolarkiewicz, P., and R. Rotunno, 1989: Low Froude number flows past three-dimensional obstacles. Part I: Baroclinically generated lee vortices. *J. Atmos. Sci.,* **46,** 1154–1164.

Wang, S.-T., 1980: Prediction of the behavior and strength of typhoons in Taiwan and its vicinity (in Chinese). National Science Council Research Rep. 108, Taipei, Taiwan, 100 pp.

Wu, C.-C., 2001: Numerical simulation of Typhoon Gladys (1994) and its interaction with Taiwan terrain using the GFDL hurricane model. *Mon. Wea. Rev.,* **129,** 1533–1549.

——, and Y.-H. Kuo, 1999: Typhoons affecting Taiwan: Current understanding and future challenges. *Bull. Amer. Meteor. Soc.,* **80,** 67–80.

——, T.-H. Yeh, Y.-H. Kuo, and W. Wang, 2002: Rainfall simulation associated with Typhoon Herb (1996) near Taiwan. Part I: The topographic effect. *Wea. Forecasting,* **17,** 1001–1015.

——, K.-H. Chou, H.-J. Cheng, and Y. Wang, 2003a: Eyewall contraction, breakdown and reformation in a landfalling typhoon. *Geophys. Res. Lett.,* **30,** 1887, doi:10.1029/2003GL017653.

——, T.-S. Huang, W.-P. Huang, and K.-H. Chou, 2003b: A new look at the binary interaction: Potential vorticity diagnosis of the unusual southward movement of Typhoon Bopha (2000) and its interaction with Typhoon Saomai (2000). *Mon. Wea. Rev.,* **131,** 1289–1300.

——, H.-J. Cheng, Y. Wang, and K.-H. Chou, 2009a: A numerical investigation of the eyewall evolution in a landfalling typhoon. *Mon. Wea. Rev.,* **137,** 21–40.

——, K. K. W. Cheung, and Y.-Y. Lo, 2009b: Numerical study of the rainfall event due to interaction of Typhoon Babs (1998) and the northeasterly monsoon. *Mon. Wea. Rev.,* **137,** 2049–2064.

Yeh, T.-C., and R. L. Elsberry, 1993a: Interaction of typhoons with the Taiwan orography. Part I: Upstream track deflection. *Mon. Wea. Rev.,* **121,** 3193–3212.

——, and ——, 1993b: Interaction of typhoons with the Taiwan orography. Part II: Continuous and discontinuous tracks across the island. *Mon. Wea. Rev.,* **121,** 3213–3233.

Zhang, D.-L., and R. A. Anthes, 1982: A high-resolution model of the planetary boundary layer—Sensitivity tests and comparisons with SESAME-79 data. *J. Appl. Meteor.,* **21,** 1594–1609.